Chemical Physics Letters 761 (2020) 138009

Contents lists available at ScienceDirect

Chemical Physics Letters

journal homepage: www.elsevier.com/locate/cplett

Research paper

Graphene quantum dots/ZnO nanocomposite: Synthesis, characterization, mechanistic investigations of photocatalytic and antibacterial activities

S. Sheik Mydeen [a,e], R. Raj Kumar [b], R. Sivakumar [a], S. Sambathkumar [c], M. Kottaisamy [d], V. S. Vasantha [e,*]

[a] Department of Chemistry, Sethu Institute of Technology, Kariapatti, Pulloor 626115, Tamil Nadu, India
[b] Institute of Medical Engineering, Department of Biophysics, School of Basic Medical Sciences, Health Science Center, Xi'an Jiaotong University, No 76 Yanta West Road, Xi'an 710061, Shaanxi, PR China
[c] Department of Chemistry, Vivekanandha College of Arts and Sciences for Women (Autonomous), Tiruchengode, Namakal 637 205, Tamil Nadu, India
[d] Department of Chemistry, Thiagarajar College of Engineering, Madurai 625015, Tamil Nadu, India
[e] School of Chemistry, Madurai Kamaraj University, Palkalainagar, Madurai 625021, Tamil Nadu, India

ARTICLE INFO

Keywords:
ZnO
Graphene quantum dots
Photocatalysis
Reactive oxygen species
Antibacterial activity

ABSTRACT

A new nanocomposite of the type ZnO fence with graphene quantum dots GQD/ZnO has been synthesized by the hydrothermal method. The crystallinity, structural and morphological properties are characterized by XRD, FT-IR, Raman, FESEM, TEM, DRS and PL techniques. Interestingly, the prepared GQD/ZnO nanocomposites act as photocatalyst for the degradation of the phenol solution with a maximum of 79% under UV light irradiation. The effect of pH for photodegradation of the catalyst has also been investigated in detail. Further, the antibacterial activity of GQD/ZnO has been investigated against *P. aeruginosa* and the results show enhanced activity, even at low concentration.

1. Introduction

Graphene belongs to renowned carbon nanomaterials, which have received much attention due to their remarkable electrical and mechanical properties that can be exploited to improve the properties of host materials for various applications [1–4]. Graphene is a two-dimensional platelet which comprises carbon atoms that are tightly packed in the honey-comb like structure. Semiconductor-mediated photocatalysis has attracted worldwide attention for its potential in environmental and energy-related applications [5–8]. Carbon–semiconductor based hybrid materials become a new class of photocatalysts, which has recently attracted lots of attention. However, the rapid recombination rate of photogenerated electron–hole pairs within photocatalytic materials results in its low efficiency, thus limiting its practical applications. Therefore, the suppression of recombination of charge carriers is the key to the enhancement of photocatalytic activity of semiconductor photocatalysts [9–13]. Recently, functionalized graphene-based semiconductor photocatalysts have attracted a lot of attention due to their good electron conductivity, large specific surface area, and high adsorption [14–19].

During the past decade, a variety of strategies have been employed to increase the photocatalytic performance of semiconductor photocatalysts, for example, *via* suitable textural design [20–25], doping [6,26–28], noble metal loading [29–31] and forming semiconductor composites [32,33]. Furthermore, the semiconductor has been made to combine graphene to form photocatalyst composite material to improve their photo-catalytic performance [16–18,34–36]. The ZnO based nanomaterial has been broadly studied, due to their excellent properties such as high redox potential, nontoxicity, low cost, and environmentally friendly feature [37,38]. Even though ZnO creates a band gap (3.37 eV) and great exciton binding energy (60 meV) [39], the small size nanoparticles have a larger surface area compared to bulk particles. This dissimilar property is used in many application fields such as nanomedicine, bio-nanotechnology, and biosensor, etc. However, photocatalyst action of ZnO is moderate under UV or sunlight, due to the quick recombination of the excited electron from the conduction band to the valence band [40]. To overcome such difficulties, modification of morphological change, surface defects, creating oxygen vacancies, doping or preparing composite material, and finally tuning the band gap of semiconductor material [41] have been conducted.

The synergistic effect of ZnO nanorods on photocatalytic performance and biological activity of graphene nano sheets has been reported

* Corresponding author.
E-mail address: vasantham999@yahoo.co.in (V.S. Vasantha).

https://doi.org/10.1016/j.cplett.2020.138009
Received 29 July 2020; Received in revised form 12 September 2020; Accepted 15 September 2020
Available online 23 September 2020

recently by A.F.Ghanem *et al* [42]. Graphene oxide/TiO_2composite are synthesized and their photocatalytic degradation against Rhodamine B and acid green 25 dyes has also been studied by M.S.Adly *et al* [43]. In 2017, M. Yadav *et al* reported the rGO/W-doped TiO_2 composite by the sol–gel method and reduction of GO was carried out with the help of TiO_2 in UV light. The efficiency of the composite was evaluated by degrading an organic pollutant (p-nitrophenol) in the presence of light [44]. X. Wan and his co-workers have described that the Nano-silicon/graphene composites are synthesized directly from silicon and graphite mixture as the raw materials with a one-step process under atmospheric pressure by the thermal plasma approach [45]. Nithya and co-workers reported on Chitoson-silver nanocomposite, green synthesized without the aid of any external chemical reducing agents studied their surface plasmonic effect, photocatalytic, and antibacterial activity in detail [46]. Green and facile synthesis of graphene nanosheets/$K_3PW_{12}O_{40}$ nanocomposites with enhanced photocatalytic activities has been reported by H.Yang *et al* [47]. Zirconium substituted magnesium, cobalt ferrite ($ZrxMg_{0.2-x}Co_{0.8-x}Fe_2O_4$) nanoparticles, and their nano-hetero-structures with graphene are synthesized by co-precipitation and ultra-sonication route respectively by A. Shabbir *et al* [48]. Many important research findings have reported entitled graphene-based semiconductor photocatalysts and consequently, GQD/ZnO nanocomposite, which has a dual function of photocatalytic and antibacterial action, has been taken for the present research.

In the present research, the nanocomposite (GQD/ZnO) namely GQD makes a fence as a decorated on ZnO has been prepared by the hydrothermal method. The synthesized nanocomposite GQD/ZnO and ZnO are subsequently characterized by XRD, FT-IR, Raman, FESEM, TEM, DRS, and PL techniques. Further, the photocatalytic activity of GQD/ZnO was investigated under UV light radiation for the degradation of phenol with various pH solutions. In addition, the antibacterial activity of both GQD/ZnO nanocomposite and pure ZnO nanoparticles has been carried out in dark condition and the mechanism of action against *Pseudomonas aeruginosa* bacteria has also been studied in detail.

2. Experimental section

2.1. Materials

Zinc acetate dihydrate (99%), Cetrimide (99%), Citric acid (99%) and sodium hydroxide (NaOH) have been purchased from Merck chemicals. All the other chemicals used are of analytical grade purchased from Merck chemicals.

2.2. Preparation of GQD/ZnO

GQD/ZnO nanocomposite was synthesized by the following literature procedure [49]. In short, 0.001 M of citric acid was put in a beaker and heated to melt at 200 °C using a heating mantle. After 25–30 mins, the orange color was formed indicating the formation of graphene quantum dots. The pH of this solution was adjusted to 7 using 1.5 M solution of NaOH. This solution was added with a mixture containing 0.02 M of Zinc acetate and 0.0005 M of cetrimide and dissolved in 30 mL of double distilled (DD) water. Then, it was stirred for an hour. In this solution, 0.05 M of NaOH was dissolved slowly in 25 mL of DD water and allowed to stir for an hour. Then, the mixed solution was moved to Teflon lined autoclave and heated for 5 hrs at 170°C. The resulting precipitate was finally filtered and washed several times with water and ethanol and dried at 60°C. Finally, the sample was annealed at the 350°C in a muffle furnace for 2 hrs and it was labeled as GQD/ZnO. The same procedure was followed for the preparation of pure zinc oxide as shown in Fig. 1.

2.3. Characterization techniques

X-ray diffraction measurements were carried out using PAN diagnostic X'Pert Pro with Cu Kα radiation (λ = 1.5418 Å) using 20 mA, with an accelerating voltage of 40 kV at a scanning rate of 2°/min. Raman spectra were recorded using Micro-Laser Raman (Seiki, Japan). The chemical nature of the sample was analyzed using SHIMADZU 8400 FT-IR Spectrometer using KBr pellet method. Morphology and microstructure investigation of the samples were carried out using a JEOL JSM-6380 LV scanning electron microscope (FESEM), operated at an accelerating voltage of 20 kV provided with Energy Dispersive Spectroscopy (EDS). Transmission electron microscopic images were taken using JEOL/JEM 1200 EX II. UV–Vis Diffuse Reflectance spectra (DRS) were recorded on a Shimadzu UV-2450 Spectrophotometer equipped with an integrating sphere. The photoluminescence spectra were recorded using a Varian Cary Eclipse photoluminescence spectrophotometer.

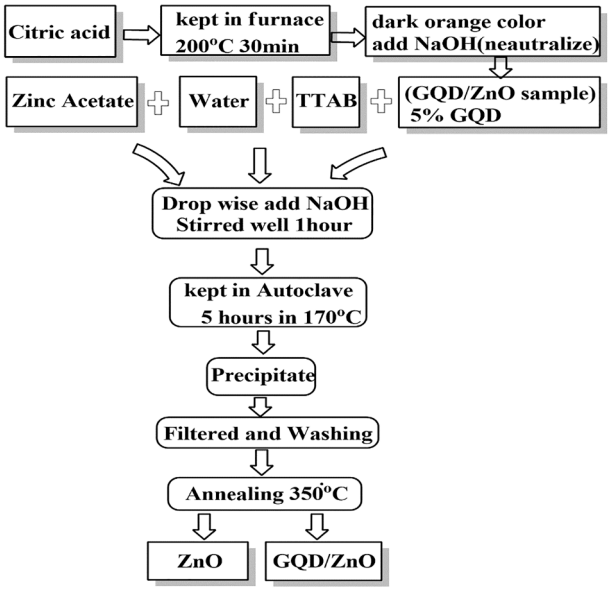

Fig. 1. Flow chart for the preparation of ZnO and GQD/ZnO nanocomposite.

2.4. Photocatalytic experiments

The photo-catalytic experiments were carried out in a cylindrical reactor (100 mL) with continuous stirring under UV light (365 nm, Hg lamp, 30 Watts). In short, 100 mg/L of phenol was taken in a 100 mL reactor and lg/L of catalyst was added. Then, the solution was kept in dark condition for 30 mins to reach adsorption equilibrium. After this, photo-catalytic degradation was started by turning on the UV light illumination. UV–Vis absorption spectra of phenol were monitored at 270 nm by taking 5 mL of the samples for every 30 mins.

2.5. Antibacterial activity

The antibacterial studies of the GQD/ZnO and ZnO were analysed against gram-negative bacteria of *Pseudomonas aeruginosa* by agar disc diffusion method. The Minimal Inhibitory Concentrations (MIC) of testing volatile portions was resolved by utilizing Mueller Hinton broth (LB) dilution strategy with Tween 80 (5%). The tubes of LB containing extracts of different concentrations were vaccinated with 10 mL of 10^{-5} CFU/mL of standardized microorganism suspensions. Control tubes without testing samples were tried, all the while. All preliminaries were done in triple time estimation of normal one. The antibacterial activity behavior of ZnO and GQD/ZnO was carried out against *P. aeruginosa* cultured using the nutrient broth for 24 h at 310 K. Disc plates were incubated day and night and then, inhibition was measured on the next day. After the effects of MIC investigation, the tube demonstrating a total absence of development was identified and incubated at standard

time and temperatures. The zone of inhibition distance was measured by vernier caliper in millimeters.

3. Results and discussion

3.1. XRD analysis

Fig. 2 shows the X-ray diffraction patterns of GQD/ZnO nanocomposites and bare ZnO samples in the range 2θ = 20-80°. The diffraction peaks observed at 2θ values 31.8°, 34.5°, 36.3°, 47.6°, 56.6°, 62.9°, 66.4°, 67.9° and 69.1° correspond to (1 0 0), (0 0 2), (1 0 1), (1 0 2), (1 1 0), (1 0 3), (2 0 0), (1 1 2) and (2 0 1) planes of ZnO. All the diffraction peaks in the XRD pattern of pure ZnO nanoparticles match well with the hexagonal phase of wurtzite ZnO [JCPDS No. 36-1451]. The 2θ values observed for GQD/ZnO nanocomposite was found to be the same for the pure ZnO, except the marginal changes in the intensity of the peaks. The diffraction peak observed at 2θ values, 25.5° and 43.2° for GQD/ZnO corresponds to (0 0 2) and (1 0 0) plane for GQD, indicating the presence of GQD in GQD/ZnO nanocomposite (Fig. 2) [50–52]. The weakened peaks of ZnO in GQD/ZnO nanocomposite compared to bare ZnO indicate that the addition of GQD induces the defects in a crystal which is probably connected with the lattice disorder and strain induced in the ZnO lattice [53]. In addition, the crystal defect of GQD/ZnO is higher in addition to GQD as indicate in the peak 101 in Fig. 2. The crystallite sizes of ZnO and GQD/ZnO nanocomposite calculated from the Scherrer's formula are found to be 73 nm and 65 nm, respectively. The dislocation density and micro-strain have been calculated for ZnO and GQD/ZnO nanocomposite and displayed in Table 1.

3.2. FT-IR spectral analysis

The chemical nature of ZnO and GQD/ZnO nanocomposite has been studied by FT-IR spectral analysis as shown in Fig. 3. The spectrum of GQD/ZnO showed band at 512 cm^{-1} which corresponds to Zn-O stretching vibrational mode [54]. The peak at 2349 cm^{-1} is due to the absorption of atmospheric carbon dioxide. The band at 3456 $cm^{-1}$is due to O-H mode of vibration. The weak C = O stretch mode vibration observed around 1722 cm^{-1} indicates the carboxylic group [55]. These peaks indicate the decomposition of acetate group after the preparation of GQD/ZnO. The stretching mode of vibration of graphene sheet C = C is detected at 1622 cm^{-1} [56]. The peak C = C and C = O peaks are broader in GQD, when the addition of ZnO in GQD, peak reduced due to interaction of GQD and ZnO. It reveals that, the formation nanocomposites show all the corresponding bands of GQD/ZnO and they indicate that the functional groups are responsible for this interaction between ZnO and GQD. The introduction of GQD fence on ZnO which can be attributed to the synergistic interaction between semiconductor and graphene support [57].

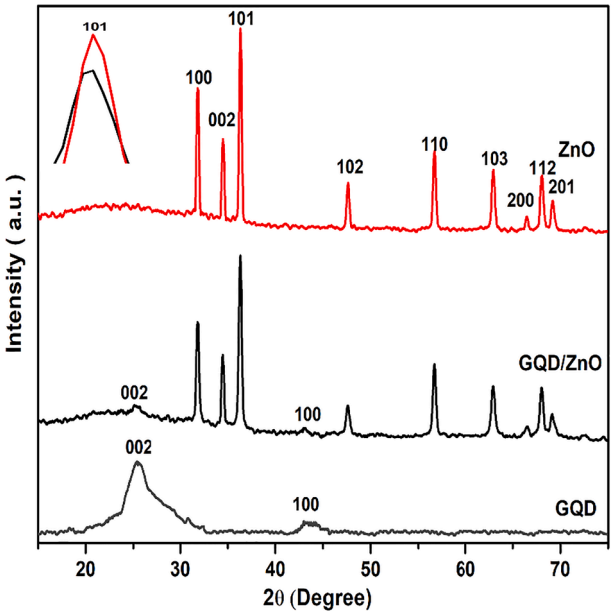

Fig. 2. XRD patterns of GQD, ZnO and GQD/ZnO nanocomposite.

Table 1
XRD parameters of pure and GQD/ZnO nanocomposite.

Samples	Crystallite size D = 0.9λ/βcosθ (nm)	Dislocation density $\delta = 1/D^2$ (x 10^{14} Lines/m^2)	Micro strain ε = βcosθ/4 (x 10^{-4})
ZnO	73	3.214	4.933
GQD/ ZnO	65	3.976	5.404

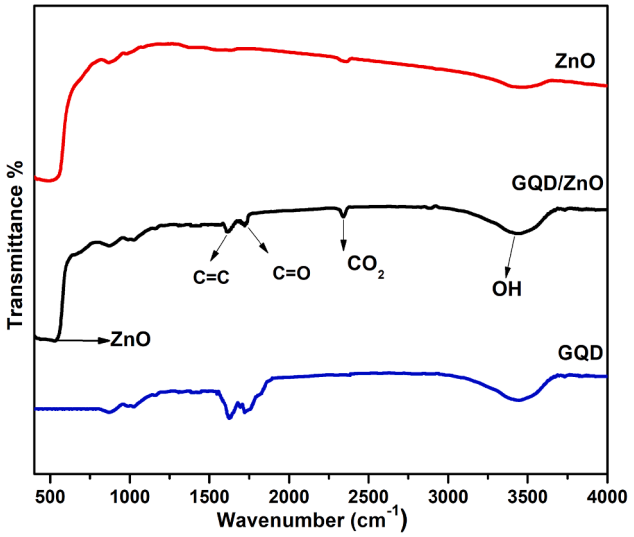

Fig. 3. FT-IR spectra of ZnO and GQD/ZnO nanocomposite.

3.3. Raman analysis

Raman spectra of pure ZnO and GQD/ZnO nanocomposite are shown in Fig. 4. The characteristic peaks of GQD are observed at 1340 and 1580 cm^{-1} of GQD/ZnO represented D-band (disordered sp^2 carbon)

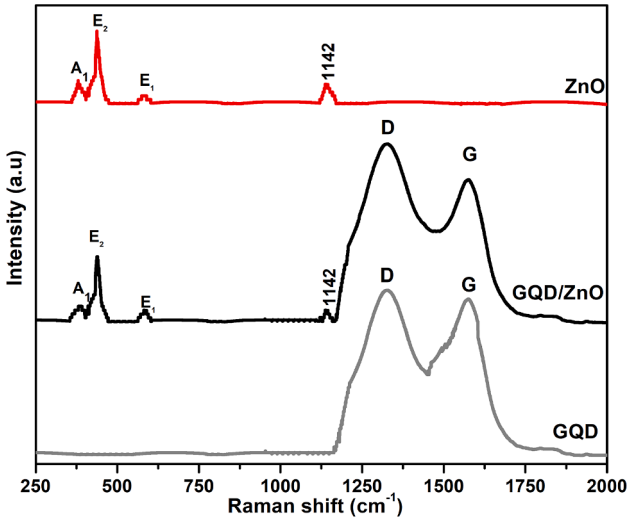

Fig. 4. Raman spectra of ZnO and GQD/ZnO nanocomposite.

and other G-band (ordered graphite), respectively. The peak intensity ratio of D-band to G-band, which is a measure of the disorder, is found to be 1.02, 1.2 for GQD and GQD/ZnO, respectively, This intensity ratio increase due to the decrease in the size of sp^2 hybridization reduction. It reveals that interaction between ZnO and graphene sheets and also it confirms the formation of GQD sheets. Meanwhile, the phonon modes of pure ZnO are observed in the range of 1142 cm^{-1}. Here, the intensity of this peak in GQD/ZnO is lower than ZnO. The ZnO peak observed at 437 cm^{-1}, corresponding to the high frequency mode of E_2 of wurtzite structure, but GQD/ZnO peak somewhat lowered by the interaction of the graphene with the ZnO. The structural defects in ZnO are represented by the peak at 583 cm^{-1}, and a small shoulder peak at 384 cm^{-1}, which is assigned to E_1 longitudinal optical (LO) mode and A_1 transverse optical (TO) mode frequencies, respectively [58]. The GQD/ZnO nanocomposite holds all the characteristic peaks of graphene and ZnO and it further provides evidence for the formation of GQD/ZnO nanocomposite.

3.4. Morphological analysis

The morphological features of both ZnO and GQD/ZnO nanocomposite were analyzed by FESEM and TEM and the representative surface micrographs are shown in Fig. 5. From the FESEM images, it can be seen that the bare ZnO and GQD/ZnO have a smooth and spherical shaped particle, though some agglomerations are observed in some parts (Fig. 5a and b). TEM images of bare ZnO nanoparticles reveal the uniform crystallite size of hexagonal wurtzite structures in Fig. 5c. This observation also complements with the XRD results. After making nanocomposite, the GQD makes a fence as a decoration on ZnO nanoparticles. Because, ZnO has electro negative element of 'O' and graphene have sp^2 hybridization with a mobile π bond electron, form a bond between ZnO and GQD. So, the result indicates that the ZnO nanoparticles are well bound with graphene quantum dots, as shown in Fig. 5d.

3.5. Optical study

The prepared catalyst is subjected to UV–Vis diffuse reflectance analysis to find the band gap of the photocatalyst. The UV–Vis absorption spectra of GQD/ZnO and ZnO reveal as the typical absorption onset at 385 and 384 nm, and extends up to 360 nm, as shown in Fig. 6 (a), respectively. Tauc plot is used to calculate the direct band gap using the formula $E_{gap} = h\nu/\lambda$ and $h\nu\alpha \propto (h\nu - E_{gap})^n$ and it is found to be 3.25 eV for GQD/ZnO and 3.20 eV for ZnO. The ZnO band gap is somewhat tuned due to the addition of graphene quantum dots in GQD/ZnO as shown in Fig. 6 (b). A transition graph of indirect band gap values of 3.16, 3.17 eV for GQD/ZnO and ZnO, respectively, are shown in Fig. 6 (c), [59]. There is no more change in the value of direct and indirect band gaps of ZnO materials. It reveals that the indirect band gap of both the sample momentum of electron energy state is the same in the conduction and valence band, but it can be possible to convert from direct

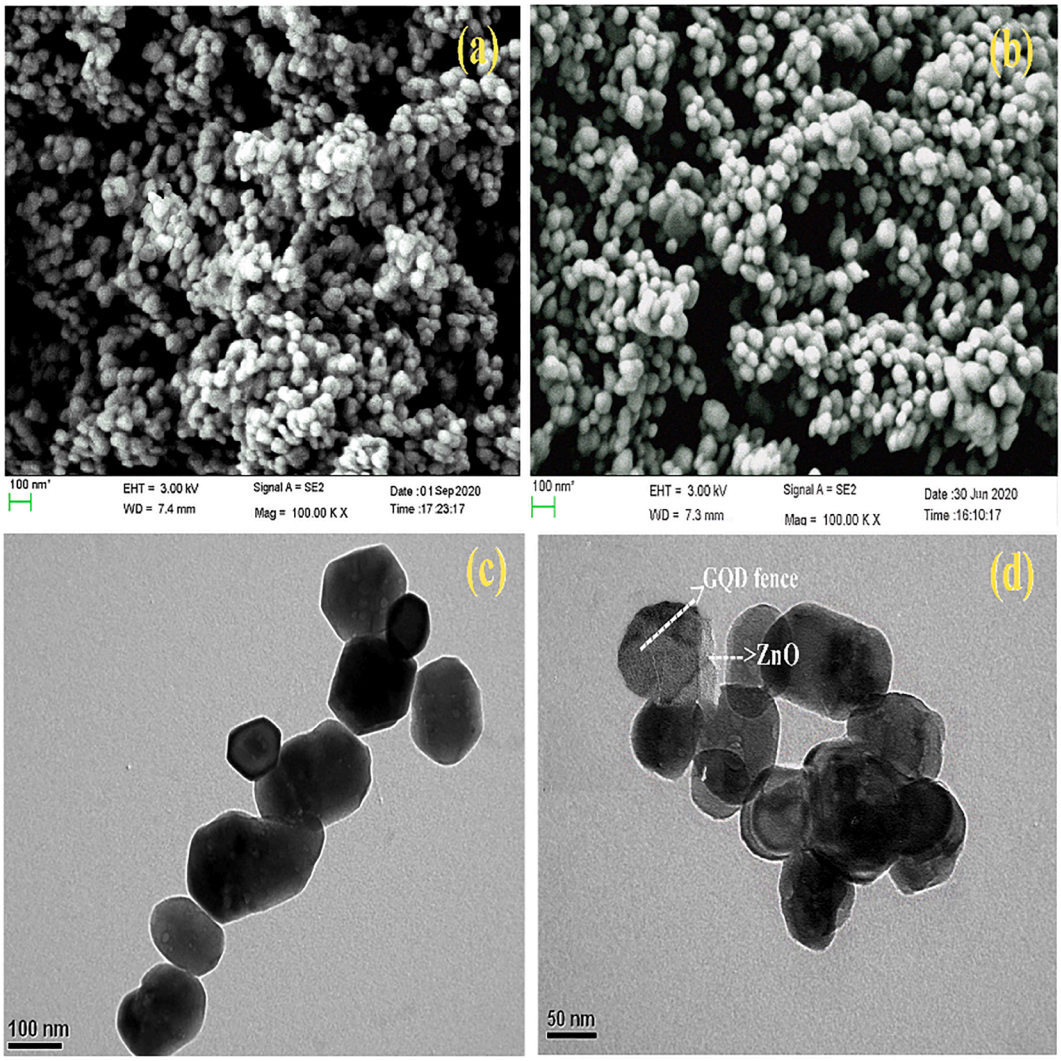

Fig. 5. FESEM images of (a) ZnO and (b) GQD/ZnO; TEM images of (c) ZnO (d) GQD/ZnO nanocomposite.

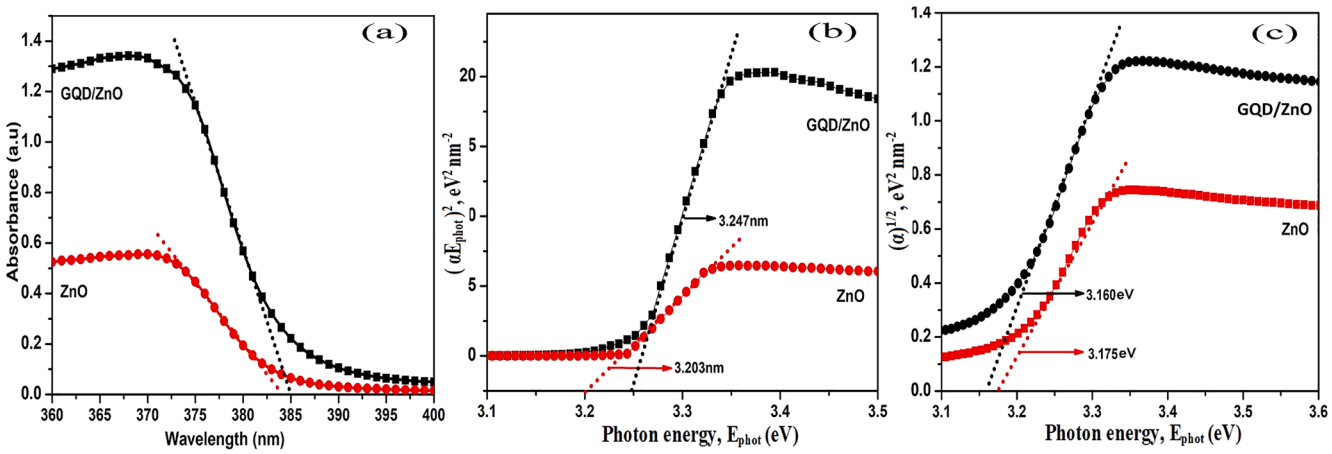

Fig. 6. (a) UV-DRS-absorbance (b) Direct band gap (c) Indirect band gap of ZnO and GQD/ZnO nanocomposite.

band to indirect band by applying an electric field [60].

3.6. Photoluminescence studies

The Photoluminescence emission spectra of GQD/ZnO and ZnO nanocomposite are recorded at room temperature at an excitation wavelength of 325 nm. The luminescence spectrum exhibit emissions at 401, 444, 488 and 520 nm, respectively, as shown in Fig. 7. [61]. The emission peak at 401 nm is attributed to the exciton recombination identified with the closest band edge emission of the ZnO [62]. The emission band at 444 nm is attributed to the violet emission which arises from the zinc interstitial defects. The next lower energy absorption bands such as blue 488 and green 520 nm emission bands are attributed to the surface conditions of the oxygen vacancy position in ZnO. The emission intensity of GQD/ZnO diminishes compared to pure ZnO by indicating that the excited electrons are transferred to the graphene quantum dots and it retards the exciton recombination in ZnO [63,64].

3.7. Photocatalytic activity

The efficiency of the GQD/ZnO nanocomposite has been evaluated against the degradation of phenol under UV radiation. The various processes of pure ZnO, GQD/ZnO and absence of catalyst in the reduction of the organic compound of phenol are initially evaluated and the quantity of catalyst is 1 g/L, pH 7.2 Further, the phenol concentration of 100 mg/L and the data of the photo-catalyst is illustrated in Fig. 8(a).

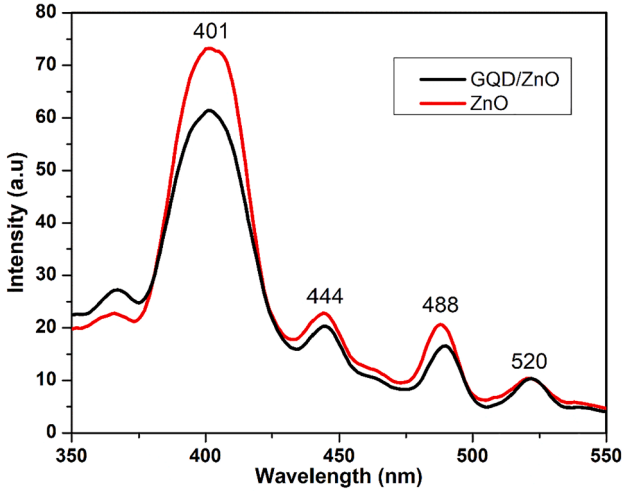

Fig. 7. PL spectra of ZnO and GQD/ZnO nanocomposites.

The degradation efficiencies of the absence of a catalyst, pure ZnO, and GQD/ZnO nanocomposite are insignificant for the degradation of a phenol molecule through adsorption. The phenol has degraded only 10% in the absence of catalyst and it can be increased in pure ZnO up to 52%, but a GQD/ZnO nanocomposite decomposition of phenol the reached rate was 79% after 4 hrs. In GQD/ZnO nanocomposites, GQD enhances the photocatalytic properties with ZnO. In this case, the presence of UV light generates electron holes in ZnO when these excited electrons are captured by GQD and then, inhibit the recombination of electron-hole pair [65].The phenol degradation has been investigated at different pH conditions on GQD/ZnO nanocomposite are as shown in Fig. 8(b). The initial pH 7.2 is then changed to pH 4.5 and 9.5 corresponding to the degradation efficiency decreased to 73% and 68%, respectively. The phenol degradation efficiency is reduced highly in acidic and alkaline medium, but it has favored in neutral pH. The pH may have affected the catalyst surface adsorption capability of phenol where as it is an important consideration of photocatalytic degradation of phenol [66].

The point zero charges of at different pH (pHpzc) of the ZnO catalyst range is at 9.0 ± 0.1 [67]. So, the catalyst surface is in positive charge condition at pH < pHpzc, negatively charge condition at pH > pHpzc, and another neutral condition at pH = pHpzc.

$$ZnO + H^+ \rightarrow ZnOH^+$$

$$ZnO + OH^- \rightarrow ZnO(OH)^-$$

Where, ZnO, $ZnOH^+$ and $ZnO(OH)^-$ are the neutral, positive, and negative groups, respectively. This property not only affects adsorption significantly, but also depends on pollutant property. In aqueous media, pollutant phenol has a pKa value 9.9 at 25 °C and it indicates that the solution at pH < PKa, a phenol structure occurs in the molecular form of C_6H_5OH. But, at pH > PKa, the phenol is de-protanate and becomes a negatively charged form of $C_6H_5O^-(ph^-)$ [68]. As a result, the adsorption depends on electric charge of both substrate and catalyst. The affinity of phenol is higher than pH 9.5 and $ZnO(OH)^-$ and (ph^-) ions are negative charge repulsion between both substrate and catalyst. So, the neutral medium is pH 7.2, the higher affinity of phenol occurs on the catalyst and finally, the degradation is higher in neutral medium. But in acidic medium, pH 4.5 slightly decreases due to positive charge $ZnOH^+$ and phenol.

Table 2 shows some reported metal oxide nanoparticles and nanocomposite for photocatalytic degradation of phenol is tabulated and the degradation rate of the catalyst mainly depends on catalyst loading, pH, phenol concentration, time and UV light.

3.7.1. Recycling of the catalyst

The reusability of both the catalysts for phenol photodegradation

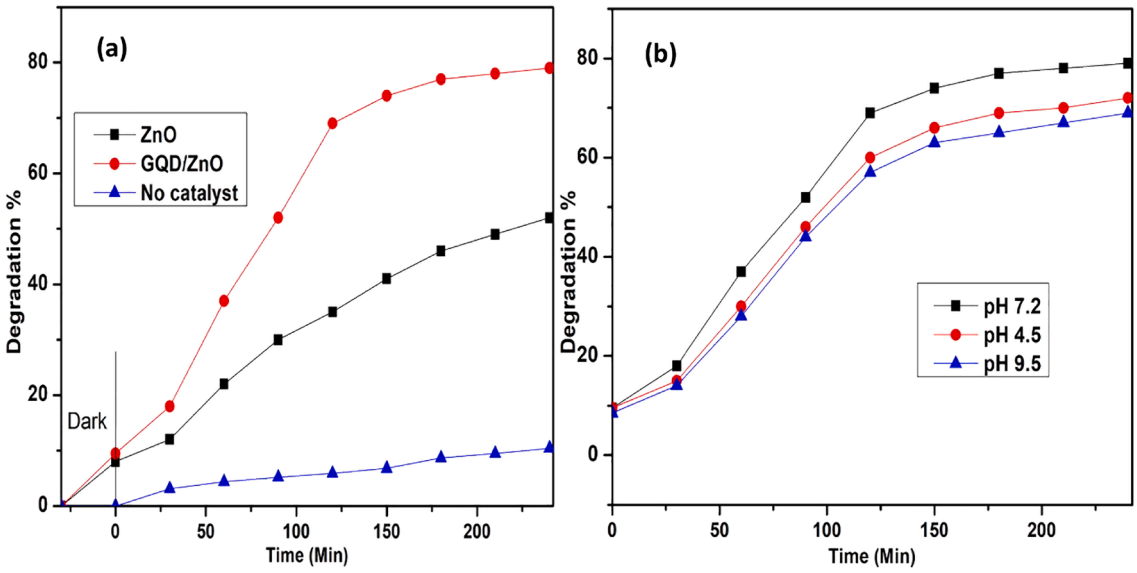

Fig. 8. (a) Photocatalytic activity of GQD/ZnO, and pure ZnO degrades phenol under UV light irradiation (phenol 0.1 g/L, catalyst 1 g/L and pH = 7.2). (b) The effect of the pH on the photocatalytic degradation of phenol by GQD/ZnO.

Table 2
Studies with some metal oxide nanocomposite for the Phenol degradation.

Catalyst	Phenol Concentration with pH	Light source	Degradation rate & Time	Ref.
TiO_2/Gr/ 30PW = 1 g/L,	50 mg/L, pH = 3.2,	Visible light (100 W tungsten lamp)	91%, achieved in 6 h	[65]
ZnO/MMT/ UV/H_2O_2 = 1 g/L	30 mg/L, pH = 6.97	UV light (254 nm, Philips 40 W UVC lamp)	80.9%, achieved in 4 h	[69]
7.5% GZnTi = 0.6 g/L	60 mg/L, pH = 4	UV light (254 nm, Philips 40 W UVC lamp)	100%, achieved in 160 min	[70]
ZnO/ rGO,70 °C = 100 mg/ L	0.1 mg/L, pH = 4	Sunlight	100%, achieved in 20 mins	[71]
ZnO, =1.5 g/ L	200 mg/L, pH = 2.5	UV light (125 W UV lamps, Black light Mercury HgV).	60%, achieved in 120 mins	[72]
GO/TiO_2 = 1.48 g/L	14.4 mg/L, pH = 6.10	UV light (254 nm, two 8 W UVC lamps)	100%, achieved in 180 mins	[73]
GQD/ZnO = 1 g/L	100 mg/L, pH = 7.2	UV light (365 nm, Philips 30 W lamp)	79%, achieved in 4 h	Present work

under UV light has been represented in Fig. 9. After each cycle, the phenol concentration is adjusted to the initial concentration of both the catalysts. The GQD/ZnO Sample dye degradation activity is gradually decreased from the third cycle compared to ZnO. But, the ZnO sample is minor and gradually decreases the activity from the 2nd cycle to the fourth cycle. The reusability of phenol degradation of GQD/ZnO sample gets good stability upto fourth cycle because the degradation rate decreased by 3.5% in the fourth cycle. Furthermore, in order to investigate the crystalline structure of GQD/ZnO after four cycles, the XRD has been tested again. The final observation of all characteristic peak positions and intensities are the same as in Fig. 2 and even the crystal structure are unchanged after four cycles. Therefore, the as-prepared GQD/ZnO nanocomposite has a good reusable quality and it is a highly stable catalyst in the practical benefits like wastewater treatment.

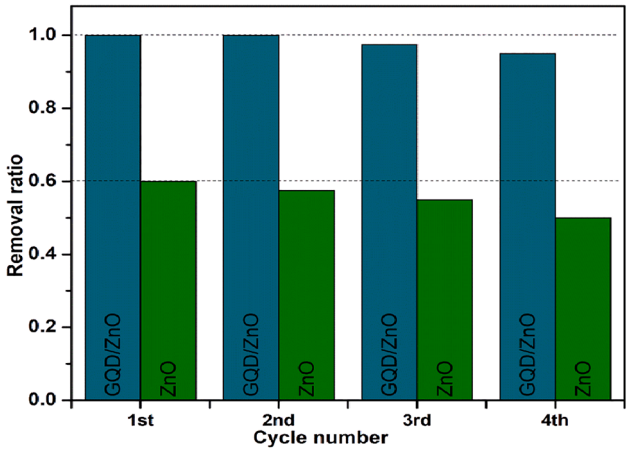

Fig. 9. Reusability results of the ZnO and GQD/ZnO in the phenol removal process under during the consecutive four cycles.

3.8. Antimicrobial activity

Antibacterial studies were carried out against *Pseudomonas aeruginosa* due to its better reaction towards nano-ZnO in our previous work [74]. The antibacterial activities of both GQD/ZnO and ZnO are performed against *P. aeruginosa* with Tetracycline as standard. The concentrations of the nanocomposite are varied between 1 mg and 1 pg and the graph is plotted against MIC values with different concentrations (Fig. 10). The result has revealed that GQD/ZnO has better antibacterial activity compared to ZnO and standard.

3.8.1. Reactivity of Zn^{2+} ion- microbe's interaction mechanism

The bacteria *P. aeruginosa* contains outer layer flagella, helical like structure which can help for the locomotion of bacteria as shown in Fig. 11. In the course of the antibacterial action of ZnO, dissolved ZnO forms Zn^{2+} ion which interacts bacteria pilus at the time of bacteria moving from one place to another under dark condition. This pilus is a rigid fiber and contains a protein that protrudes the bacterial cell surface. The outer membrane of gram-negative bacteria contain lipoteichoic acid, which contain a high amount of polyphosphate anion, creates a negatively charged cell wall in the outer membrane of bacteria,

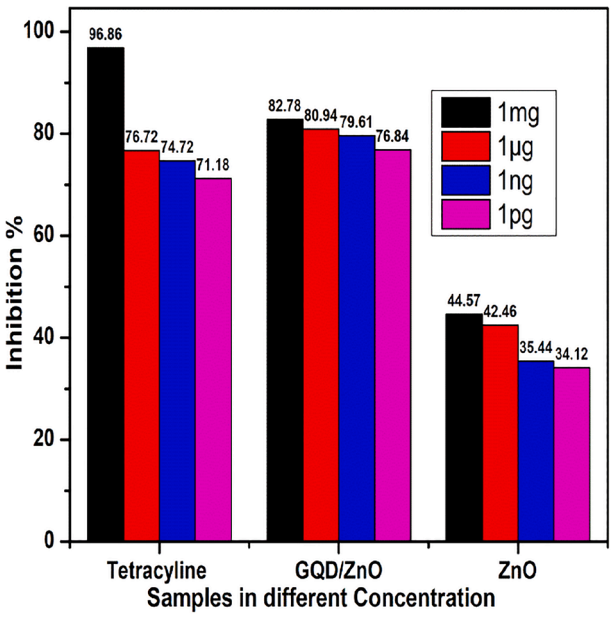

Fig. 10. Antibacterial activities of the ZnO and GQD/ZnO nanocomposite.

thereby, the Zn^{2+} ion is attracted by polyphosphate anion of the outer membrane [75,76]. In bacteria, active transports of vitamins, minerals, and ions are formed in the form of diffusion method and for this reason, the bacteria produce ATP. Cytoplasmic zone is present in between the outer and inner membrane and consists of a thin layer of peptidoglycan which possesses a gel similar regularity. Such a peptidoglycan layer helps allow and transport sugars, amino acids, and other ions into the cells. Here, the transition metal ion diffuses the outer membrane to the inner cytoplasmic membrane reaching through the peptidoglycan mechanism which has not yet been clearly explained. When the Zn^{2+} ion is absorbed by peptidoglycan (PGN), it induces the initiations of the production of autolysins. This excessive production of autolysins subsequently induces the dramatic autolysin mediated lysis and this process has been considered to enhance the inhibitions of peptidoglycan elongation with bacteriolysis and the destruction of *P. aeruginosa* peptidoglycan cell wall [77]. Then, the diffusion of Zn^{2+} ion through the cytoplasm reaches to the ribosome and mitochondria. Zn^{2+} ion reduces the activity of protein synthesis from the ribosome and prevents Nicotinamide Adenine Dinucleotide Hydrogen (NADH) activity in mitochondria. Furthermore, the NADH activity of an electron carrier, energy production and distribute energy in all parts of the body are inhibited [78]. Both ZnO and GQD/ZnO samples after dissolution to form Zn^{2+} ions move through the outer membrane or Porin to reach cytoplasmic and then, kill the chromosomes of bacteria cell.

3.8.2. Mechanism of ROS

In a solution medium, ZnO nano materials move from the bacterial cells with the help of osmotic pressure. Aerobic bacteria get energy from respiration, using molecular oxygen (O_2) or oxidation of nutrients. The bacterial cell promotes oxidative stress and it is induced when diffused ZnO generates antimicrobial activity mechanism [79]. As a result, the reduction of oxygen molecules causes oxygen demand forming in bacteria cells. The surface of nanoparticles crystal has oxygen defect sites which can enhance Reactive Oxygen Species (ROS) production and antibacterial activity in dark condition [80]. From PL data, sample GQD/ZnO nanocomposite electrons are excited and quick recombination level inhibition occurs better than ZnO. These excited level electrons are donated to respire oxygen besides producing super oxide of (ROS). Hence, the excited electrons are easily collected by GQD and more ROS radicals are produced. A higher concentration of ROS radical is produced in GQD/ZnO and it enhances the antibacterial activity than the ZnO. Consequently, the ROS provides an admirable antibacterial activity causing excessive damage to the inner functional group of bacteria. Hence, ROS moves through the cytoplasm and it causes damage to mitochondria, lipids, ribosome's and chromosomes. The same mechanism may be possible that specific nanoparticles enter into the inner body bacteria and then, gets energy from intracellular metabolism to make ROS radical.

At the same time, ZnO/GQD the partially excited electron moved to GQD fence and also inhibit the recombination of excited electron. This fence electrons were possibly captured by electronic acceptors adsorbed (O_2), in order to form a superoxide radical anion ($O_2^{\bullet}$), it is represented as GQD-ROS [81,82] as shown in Fig. 11. Furthermore, The production of ROS in the dark light, especially in nano ZnO, involving superoxide species facilitated by surface defects noted in PL and XRD spectra. Hence, the ZnO surface electron adsorbed (O_2), and formation of ROS radical ($O_2^{\bullet}$), it is represented as ZnO-ROS. [83–85]. Moreover, GQD

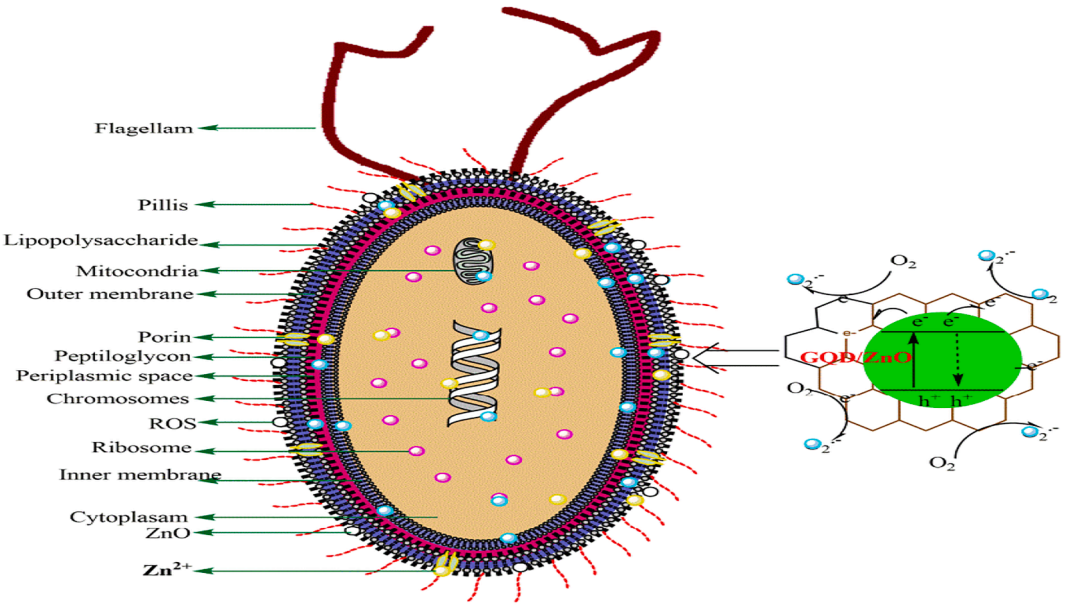

Fig. 11. Schematic illustration of ZnO and GQD/ZnO nanocomposite antibacterial mechanism of Gram-ve *Pseudomonas aeruginosa* bacteria.

interaction with bacteria functional group (COOH, OH) formation of $OH^{\bullet}$ of ROS radical, it is represented as GQD-ROS. [86]. Additionally, ZnO dissolution with solvent or bacterial acid to the formation of Zn^{2+} ion. Finally, all ROS and Zn^{2+} enter the bacteria and damage the bacteria cell. From above this mechanism GQD/ZnO sample only produces more ROS radical with help of GQD fence and enhances the antibacterial activity than ZnO. So that, the GQD/ZnO has MIC value and the lowest concentration GQD enhances the observable inhibit in the growth of bacteria [87]. Furthermore, the nanocomposite of GQD/ZnO shows higher activity than tetracycline and ZnO Compound for MIC at 1 pg/mL against *P. aeruginosa* (Fig. 10). It reveals that GQD/ZnO nanocomposites produce Zn^{2+}, GQD-ROS and ZnO-ROS to three ways possible attacks to *Pseudomonas aeruginosa* than two-way attack of Zn^{2+}, ZnO-ROS for ZnO.

4. Conclusions

In the present work, the facile syntheses of GQD/ZnO nanocomposite from the hydrothermal method are described. The characterizations of the GQD/ZnO nanocomposite are accomplished by various spectral and physico-chemical methods. The XRD and TEM images have also picturised that the ZnO sample has hexagonal particle structure and GQD/ZnO has formed GQD fence layer on ZnO. The PL spectra indicate the GQD/ZnO has graphene act as an electron sink for the accumulation of charges from defect levels of ZnO and it controls the recombination of charge carriers. Furthermore, the GQD/ZnO nanocomposite has been proved to be an effective photocatalyst for the photocatalytic activity of the degradation of phenol (79%) in aqueous media under UV light. In addition, GQD/ZnO inhibits the growth of various microorganisms markedly by exhibiting higher antimicrobial activity against Gram-negative bacteria. GQD/ZnO has followed three-way antibacterial mechanisms of Zn^{2+}, GQD-ROS, and ZnO-ROS of destroying the components of bacteria and providing an end way of killing the bacteria. But, ZnO sample follows Zn^{2+}, ZnO-ROS only. For this reason, GQD fence on ZnO has better MIC value and hence, it is used in the surface coating of medical devices and nanomedicine.

CRediT authorship contribution statement

S. Sheik Mydeen: Writing-original draft, Investigation, Methodology and Data Curation. **R. Raj Kumar:** Formal analysis, Resources, Writing-review & editing. **R. Sivakumar:** Software, Validation, Writing-original draft. **S. Sambathkumar:** Conceptualization, Validation, Visualization. **M. Kottaisamy:** Investigation, Data Curation, Validation. **V.S. Vasantha:** Project Administration, Supervision, Writing-original draft.

Declaration of Competing Interest

The authors declare that they have no known competing financial interests or personal relationships that could have appeared to influence the work reported in this paper.

Acknowledgement

The authors declare no competing financial interest.

References

[1] Q. Xiang, J. Yu, M. Jaroniec, Chem. Soc. Rev. 41 (2012) 782–796.
[2] M.D. Stoller, S. Park, Y. Zhu, J. An, R.S. Ruoff, Nano Lett. 8 (2008) 3498–3502.
[3] R. Parameshwari, K. Jothivenkatachalam, C.E. Banks, K. Jeganathan, Physica B: Condensed Matter. 506 (2017) 32–41.
[4] S. Bharech, R. Kumar, J. Mater. Sci. Mech. Engin. 2 (2015) 70–73.
[5] Q.J. Xiang, J.G. Yu, P.K. Wong, J. Colloid Interface Sci. 357 (2011) 163.
[6] J.H. Park, S. Kim, A.J. Bard, Nano Lett. 6 (2006) 24.
[7] C.H. Li, F. Wang, J.C. Yu, Energy Environ. Sci. 4 (2011) 100.
[8] G. Liu, H.G. Yang, X.W. Wang, L.N. Cheng, J. Pan, G.Q. Lu, H.M. Cheng, J. Am. Chem. Soc. 131 (2009) 12868.
[9] J.G. Yu, T.T. Ma, G. Liu, B. Cheng, Dalton Trans. 40 (2011) 6635.
[10] S.X. Min, G.X. Lu, J. Phys. Chem. C. 115 (2011) 13938.
[11] F. Wang, K. Zhang, J. Mol. Catal. A: Chem. 345 (2011) 101.
[12] C. Park, E.S. Engel, A. Crowe, T.R. Gilbert, N.M. Rodriguez, Langmuir. 16 (2000) 8050.
[13] L.L. Zhang, Z.G. Xiong, X.S. Zhao, ACS Nano. 4 (2010) 7030.
[14] A.J. Du, Y.H. Ng, N.J. Bell, Z.H. Zhu, R. Amal, S.C. Smith, J. Phys. Chem. Lett. 2 (2011) 894.
[15] R. Leary, A. Westwood, Carbon. 49 (2011) 741.
[16] I.V. Lightcap, T.H. Kosel, P.V. Kamat, Nano Lett. 10 (2010) 577.
[17] G. Williams, B. Seger, P.V. Kamat, ACS Nano. 2 (2008) 1487.
[18] H. Zhang, X.J. Lv, Y.M. Li, Y. Wang, J.H. Li, ACS Nano. 4 (2010) 380.
[19] S. Wang, B.M. Goh, K.K. Manga, Q.L. Bao, P. Yang, K.P. Loh, ACS Nano. 4 (2010) 6180.
[20] Y.W. Cheng, R.C.Y. Chan, P.K. Wong, Water Res. 41 (2007) 84.
[21] P. Panagiotopoulou, A. Christodoulakis, D.I. Kondarides, S. Boghosian, J. Catal. 240 (2006) 114.
[22] H.G. Yang, C.H. Sun, S.Z. Qiao, J. Zou, G. Liu, S.C. Smith, H.M. Cheng, G.Q. Lu, Nature 453 (2008) 638.
[23] S.I. In, Y.D. Hou, B.L. Abrams, P.C.K. Vesborg, I. Chorkendorff, J. Electrochem. Soc. 157 (2010) E69.
[24] S.W. Liu, J.G. Yu, M. Jaroniec, J. Am. Chem. Soc. 132 (2010) 11914.
[25] Q.J. Xiang, J.G. Yu, M. Jaroniec, Chem. Commun. 47 (2011) 4532.
[26] M. Ksibi, S. Rossignol, J.M. Tatibouet, C. Trapalis, Mater. Lett. 62 (2008) 4204.
[27] Q.J. Xiang, J.G. Yu, W.G. Wang, M. Jaroniec, Chem. Commun. 47 (2011) 6906.
[28] J.G. Yu, Q.J. Xiang, M.H. Zhou, Appl. Catal. B. 90 (2009) 595.
[29] J.G. Yu, J.F. Xiong, B. Cheng, S.W. Liu, Appl. Catal. B. 60 (2005) 211.
[30] J.G. Yu, L.F. Qi, M. Jaroniec, J. Phys. Chem. C. 114 (2010) 13118.
[31] Q.J. Xiang, J.G. Yu, B. Cheng, H.C. Ong, Chem.–Asian. J. 5 (2010) 1466.
[32] K. Woan, G. Pyrgiotakis, W. Sigmund, Adv. Mater. 21 (2009) 2233.
[33] J.G. Yu, J. Zhang, M. Jaroniec, Green Chem. 12 (2010) 1611.
[34] T.N. Lambert, C.A. Chavez, N.S. Bell, C.M. Washburn, D.R. Wheeler, M. T. Brumbach, Nanoscale. 3 (2011) 188.
[35] Y.P. Zhang, C.X. Pan, J. Mater. Sci. 46 (2011) 2622.
[36] B.J. Li, H.Q. Cao, J. Mater. Chem. 21 (2011) 3346.
[37] V. Revathi, K. Karthik, J. *Mater. Sci.: Mater. Electron.* 29 (2018) 18519–18530.
[38] M. Gancheva, V.M. Markova, G. Atanasova, D. Kovacheva, I. Uzunov, R. Cukeva, Appl. Surf. Sci. 368 (2016) 258–266.
[39] Z.J. Wang, Phys. Condens. Matter. (2004) 829–858.
[40] L. Yuanyuan, Z. Zhiyong, Y. Junfeng, Z. Wu, Z. Chunxue, L. Jin, J Allloy Comp. 718 (2017) 161–169.
[41] H. Liu, M. Li, J. Yang, C. Hu, J. Shang, H. Zhai, Mater Res Bull. (2018) 19–27.
[42] A.F. Ghanem, A.A. Badawy, M.E. Mohram, M.H. Abdel Rehim, Heliyon 6 (2020), e03283.
[43] M.S. Adly, S.M. El-Dafrawy, S.A. El-Hakam, J. Mater. Res. Technol. 8 (2019) 5610–5622.
[44] M. Yadav, A. Yadav, R. Fernandes, Y. Popat, M. Orlandi, A. Dashora, D.C. Kothari, A. Miotello, B.L. Ahuja, N. Patel, J. of Envir. Manag. 203 (2017) 364–374.
[45] X. Wan, Y. Fan, W. Ma, S. Li, X. Huang, J. Yu, Mate. Lett. 220 (2018) 144–147.
[46] A. Nithya, H.L. JeevaKumari, K. Rokesh, K. Ruckmani, K. Jeganathan, K. Jothivenkatachalam, J. of Photo. Photobio. B: Biology. 153 (2015) 412–422.
[47] H. Yanga, X. Liu, S. Sun, Y. Niea, H. Wua, T. Yanga, S. Zhenga, S. Lin, Mate. Rese. Bull. 78 (2016) 112–118.
[48] A. Shabbir, S. Ajmala, M. Shahidb, I. Shakirc, P.O. Agboolad, M.F. Warsia, Ceram. Int. 45 (2019) 16121–16129.
[49] Y. Dong, J. Shao, C. Chen, H. Li, R. Wang, Y. Chi, X. Lin, G. Chen, Carbon. 50 (2012) 4738–4743.
[50] Z. Chen, N. Zhang, Y.J. Xu, Cryst. Eng. Comm. 15 (2013) 3022–3030.
[51] D.I. Son, B.W. Kwon, D.H. Park, W.S. Seo, Y. Yi, B. Angadi, C.L. Lee, W.K. Choi, Nat. Nanotech. 7 (7) (2012) 465–471.
[52] M. Ding, J. Zhou, H. Yanga, R. Cao, S. Zhang, M. Shao, X. Xu, Chin. Chem. Lett. 31 (2020) 71–76.
[53] R. Karmakar, S.K. Neogi, A. Banerjee, S. Bandyopadhyay, Appl. Surf. Sci. 263 (2012) 671–677.
[54] D. Geeha, T. Thilagavathi, J. Dig, J. Nanomate. Biostruc. 5 (2010) 297–301.
[55] N. Takashi, N. Hiroshi, I. Masatou, Y. Takatoshi, H. Masataka, A. Michitaka, Clay Science. 18 (2014) 107–115.
[56] F.E. Tarko, W. Delele, W. Egyp, J. Basic Appl. Scie. 4 (2017) 74–79.
[57] H.P. Cong, X.C. Ren, P. Wang, S.H. Yu, ACS Nano. 6 (2012) 2693–2703.
[58] S. Meti, M.R. Rahman, D.I. Ahmad, K.U. Bhat, Appl. Surf. Sci. 451 (2018) 67–75.
[59] R.R. Kanna, N.R. Dhineshbabu, P. Paramasivam, V. Rajendran, R. Yuvakkumar, J. Nanosci. Nanotech. 16 (2016).
[60] S. Li, L. J-Li, Q. Jiang, G.W. Yang, J. App. Phy. 108 (2010) 24302.
[61] B.L. Atul, S.M. Yuvaraj, Saudi. Chemic. Soc. 19 (2015) 471–478.
[62] F. Xu, V. Volkov, Y. Zhu, H. Bai, A. Rea, N. Valappil, J. Phys. Chem. C. 113 (2009) 19419–19423.
[63] Y. Gu, M. Xing, J. Zhang, Appl. Surf. Sci. 3 (2014) 8–15.
[64] V.P. Chuyen, R. Sergej, T. Ralf, K. Michael, W. Stefan, E. Emre, Nanoscale. 8 (2016) 9682.
[65] E. Rafiee, E. Noori, A.A. Zinatizadeh, H. Zanganeh, RSC Adv. 6 (2016).
[66] J.C. Sin, S.M. Lam, K.T. Lee, A.R. Mohamed, Ceram. Int. 39 (2013) 5833–5843.
[67] M.M. Ba-Abbad, A.A.H. Kadhum, A.B. Mohamad, M.S. Takriff, K. Sopian Rese on Chemi. Interme. 35 (2012) 1981–1996.
[68] S.J. Royaee, M. Sohrabi, F. Soleymani, J. Chemi. Tech. Biotech. 86 (2010) 205–212.
[69] J. Ye, X. Li, J. Hong, J. Chen, Q. Fan, Mater. Scie. in Semicond. Proce. 39 (2015) 17–22.

[70] F. Hayati, A.A. Isari, M. Fattahi, B. Anvaripour, S. Jorfi, RSC Adv. 8 (2018) 40035.
[71] R. Yada, V. Kumar, V. Saxena, P. Singh, V.K. Singh, Ceram. Int. 45 (2019) 24999–25009.
[72] H. Benhebal, M. Chaib, T. Salmon, J. Geens, A. Leonard, S.D. Lambert, M. Crine, B. Heinrichs, Alexandria Engi. Jour. 52 (2013) 517–523.
[73] R. Shahbazi, A. Payan, M. Fattahi, J. Photochem. Photobio. A: Chem. 364 (2018) 564–576.
[74] S.S. Mydeen, M. Kottaisamy, V.S. Vasantha, Intern. J. of Innov. Tech. and Expl. Eng. 9 (2) (2019) 930–938.
[75] A.B. Djurisi, Y.H. Leung, A.M.C. Ng, X.Y. Xu, P.K.H. Lee, N. Degger, Small. 11 (2015) 26.
[76] V. Revathi, K. Karthik, Chemi. Data, Collections. 21 (2019), 100229.
[77] M.K. Saido, S. Saitama, K. Saitama, A revi, Annals of Microbio. Infec. Dise. 2 (2019) 2637–5346.
[78] S.S. Mark, H. Judy, JBC Papers in Press. (2006).
[79] M. Gratzel, Nature. 414 (2001) 338.
[80] K. Hirota, M. Sugimoto, M. Kato, K. Tsukagoshi, T. Tanigawa, H. Sugimoto, Ceram. Int. 36 (2010) 497.
[81] Y. Yang, M. Wu, X. Zhu, H. Xu, S. Ma, Y. Zhi, H. Xia, X. Liu, J. Pan, J.-Y. Tang, S.-P. Chai, L. Palmisano, F. Parrino, J. Liu, J. Ma, Z.L. Wang, L. Tan, Y.-F. Zhao, Y.-F. Song, P. Singh, P. Raizada, D. Jiang, D. Li, R.-A. Geioushy, J. Ma, J. Zhang, S. Hu, R. Feng, G. Liu, M. Liu, Z. Li, M. Shao, N. Li, J. Peng, W.-J. Ong, N. Kornienoko, Z. Xing, X. Fan, J. Ma, Chin. Chem. Lett. 31 (2019).
[82] V.L. Prasanna, R. Vijayaraghavan, Langmuir. 31 (2015) 9155–9162.
[83] K. Karthik, S. Dhanuskodi, S. Prabukumar, S. Sivaramakrishnan, Optik. 204 (2020), 164221.
[84] J. Gupta, D. Bahadur, ACS Omega 3 (2018) 2956–2965.
[85] Y. Wang, W. Kong, L. Wang, J.Z. Zhang, Y. Li, X. Liua, Y. Lia, Phys. Chem. Chem Phys. 21 (2019) 1336.
[86] Y. Li, W. Zhang, J. Niu, Y. Chen, ACS Nano. 26 (2012) 5164.
[87] K. Karthik, D. Radhika, S. Kishor Kumar, K.R. Reddy, A.V. Raghu, Adv. Collid. Inter. Sci. 281 (2020) 102178.